Data in Brief 42 (2022) 108059

Contents lists available at ScienceDirect

Data in Brief

journal homepage: www.elsevier.com/locate/dib

Data Article

# Crystallographic orientation data from chloride-induced stress corrosion crack (CISCC) paths in gas tungsten arc welded (GTAW) austenitic stainless steel 304L

Haozheng J. Qu*, Janelle P. Wharry

*School of Materials Engineering, Purdue University, IN, USA*

ARTICLE INFO

*Article history:*
Received 3 February 2022
Accepted 11 March 2022
Available online 17 March 2022

Dataset link: Crystallographic orientation data from chloride-induced stress corrosion crack (CISCC) paths in gas tungsten arc welded (GTAW) austenitic stainless steel 304L (Original data)

*Keywords:*
Austenitic stainless steel
Stress corrosion cracking
Transgranular cracking
Schmid Factor
Taylor Factor
Arc welding
EBSD

ABSTRACT

This Data in Brief article presents crystallographic data collected along chloride-induced stress corrosion cracks (CISCC) in a gas tungsten arc welded (GTAW) austenitic stainless steel (AuSS) 304L. The experimental setup involved a welded stainless steel 304L coupon of dimensions 105 mm × 18.5 mm × 3 mm, loaded in a 4-point bending fixture with a maximum tensile stress of 380 MPa. The fixtured specimen was immersed in boiling magnesium chloride ($MgCl_2$) solution until a through-crack was observed on the specimen surface after 17 hours of boiling. The cross-section was subsequently polished, and 37 cracks of interest in the heat affected zone (HAZ) and weld zone (WZ) were selected for crystallographic characterization. Scanning electron microscopy (SEM) based electron backscatter diffraction (EBSD) was used to map the grain orientations along and surrounding each crack path. The obtained orientation imaging microscopy (OIM) datasets were post-processed using EDAX OIM V8 proprietary software to generate inverse pole figures (IPF), image quality (IQ) figures, detector signal (SEM) images, and to determine the Taylor factor and Schmid factor of mapped grains. This dataset can be used to understand CISCC crack initiation, propagation, and termination behaviors, as has been reported

* Corresponding author at: School of Materials Engineering, Purdue University, 205 Gates Road, Flex Lab, West Lafayette, IN 47906, USA.
*E-mail address:* qu34@purdue.edu (H.J. Qu).

https://doi.org/10.1016/j.dib.2022.108059
2352-3409/© 2022 The Author(s). Published by Elsevier Inc. This is an open access article under the CC BY-NC-ND license (http://creativecommons.org/licenses/by-nc-nd/4.0/)

in the accompanying original research article. This data article providing the raw EBSD OIM datasets and processed images formatted for accessibility in future studies. This comprehensive EBSD dataset can further be used to extract grain boundary misorientation information; benchmark comparative studies of SCC/CISCC in AuSS and other Fe or Ni alloys; and provide critical validation data on grain morphology, misorientation, and crystallography for GTAW and CISCC models.

© 2022 The Author(s). Published by Elsevier Inc.
This is an open access article under the CC BY-NC-ND license (http://creativecommons.org/licenses/by-nc-nd/4.0/)

## Specifications Table

| | |
|---|---|
| Subject | Metals and Alloys |
| Specific subject area | Transgranular stress corrosion cracking of welded austenitic stainless steel 304L |
| Type of data | Table summarizing cracking behaviors for each crack (.xlsx)<br>Raw EBSD OIM dataset files (.oim)<br>EBSD grain orientation maps (.tif)<br>High-resolution SEM images of crack morphology (.tif) |
| How data were acquired | SEM: Quanta 650 FEG SEM (for EBSD mapping) and Thermo Fisher Scientific Helios G4 UX Dual Beam SEM (for high-resolution crack morphology imaging)<br>EBSD detector: Hikari$^{TM}$, EDAX<br>EBSD analysis: EDAX OIM V8 package |
| Data format | Raw: OIM, TIFF<br>Analyzed: XLSX<br>Filtered |
| Parameters for data collection | • Tensile stress from 4-point bending: 380 MPa<br>• SCC testing temperature: 155.0 $\pm$ 1.0°C<br>• Polishing: 360-1200 grit SiC paper, 0.05 $\mu$m colloidal silica vibratory polish<br>• SEM accelerating voltage, current: 20 kV, 5 nA<br>• EBSD dwell time, step size: 1 ms, 0.3-2.5 $\mu$m/pixel<br>• OIM: neighboring confidence index (CI) >0.1, neighboring grain tolerance angle 3° |
| Description of data collection | A welded stainless steel 304L coupon in a 4-point bend fixture was immersed in boiling $MgCl_2$ to induce CISCC. A cross-section of the cracked region was polished. All cracks on the cross-section were identified by scanning electron microscopy (SEM). Then, 37 cracks of interest (based primarily on their length) were selected for SEM electron backscatter diffraction (EBSD) to obtain crystallographic information along the crack path. EBSD maps were post-processed in EDAX OIM V8 software to extract crystal orientation, Schmid factor, and Taylor factor of grains along (and near) the crack paths. |
| Data source location | Institution: Purdue University<br>City/Town/Region: West Lafayette, Indiana 47906<br>Country: U.S.A.<br>Latitude and longitude: 40.42141, -86.92318 |
| Data accessibility | Examples of EBSD images are included in the article. Complete datasets are available at:<br>Repository name: Mendeley Data<br>Direct URL to data: doi: 10.17632/23wxhgd55p.5 |
| Related research article | |

## Value of the Data

- This EBSD data can be used to understand chloride-induced stress corrosion crack (CISCC) initiation, propagation, and termination behaviors in 304L stainless steel welds, and the crystallographic effects on these behaviors. This dataset also enables comparative study of SCC/CISCC in other alloys or environments, and provides key validation data for CISCC models.
- This dataset can benefit experimentalists and modelers who are investigating fundamental CISCC mechanisms, grain evolution under arc welding, and other corrosion-related phenomena.
- Future research may use the raw EBSD data to extract the effects of grain boundary misorientation or local strain and stress, on CISCC initiation and propagation in AuSS. Data may also be used to motivate advanced *in situ* experiments such as x-ray tomography, neutron scattering, or transmission electron microscopy (TEM), to inform fundamental CISCC mechanisms.
- The dataset also contains grain morphologic and crystallographic information across the weld zone and heat-affected zone, and can thus provide validation data for welding models and guide the selection of weld parameters in experiments or engineering applications.

## 1. Data Description

### *1.1. Data*

#### *1.1.1. Description of data files*

The data repository contains raw SEM EBSD files and associated image files for 37 CISCC cracks observed in GTAW 304L AuSS. All files for a given crack are organized into a dedicated folder with naming convention "***zone #***" – where "*zone*" indicates whether the crack was located in the heat-affected zone (HAZ) or the weld zone (WZ), and "#" is the identification number of the crack. The files in each of these folders are:

- ***zone #.oim*** – Raw EBSD OIM file
- ***zone IPF #.tif*** – inverse pole figure (IPF) image
- ***zone IQ #.tif*** – image quality (IQ) figure
- ***zone EBSD-SEM #.tif*** – SEM EBSD detector signal image of the crack(s)
- ***zone SEM #.tif*** –SEM image of the crack(s) with better resolution

In addition, a table ***DATA IN BRIEF crack behavior summary table. xlsx*** is also included in the repository to link the raw data and image files to key metadata including crack initiation mode, propagation mode, crack length, and other notable behaviors.

To help readers understand how to handle the aforementioned data files, examples are provided in Section 1.2.

#### *1.1.2. Working with .oim and .tif files for each crack*

Fig. 1 shows the set of corresponding IPF, IQ, and HR-SEM images for Crack #11 in the HAZ; note the scale bar is consistent throughout this composite figure. Through careful comparison of the IQ and SEM images, the crack path may be identified relative to the grain structure, and subsequently marked by black lines in Fig. 1(a). In Fig. 1(b), different grain boundary (GB) types, including $\Sigma 3$ through $\Sigma 11$ coincident site lattice (CSL) GBs, are overlaid on the IQ figure. In addition to qualitative grain orientation and GB information, quantitative data, such as Schmid factor, Taylor factor, and GB misorientation, can be accessed from the OIM files. Within each of the OIM files, Schmid factor and Taylor factor maps are readily available for further analysis.

Similarly, Fig. 2 shows the set of corresponding IPF, IQ, and HR-SEM images for example Crack #29 in the WZ. An internal pit is apparent at the intersection between the crack path and a GB throughout Fig. 2.

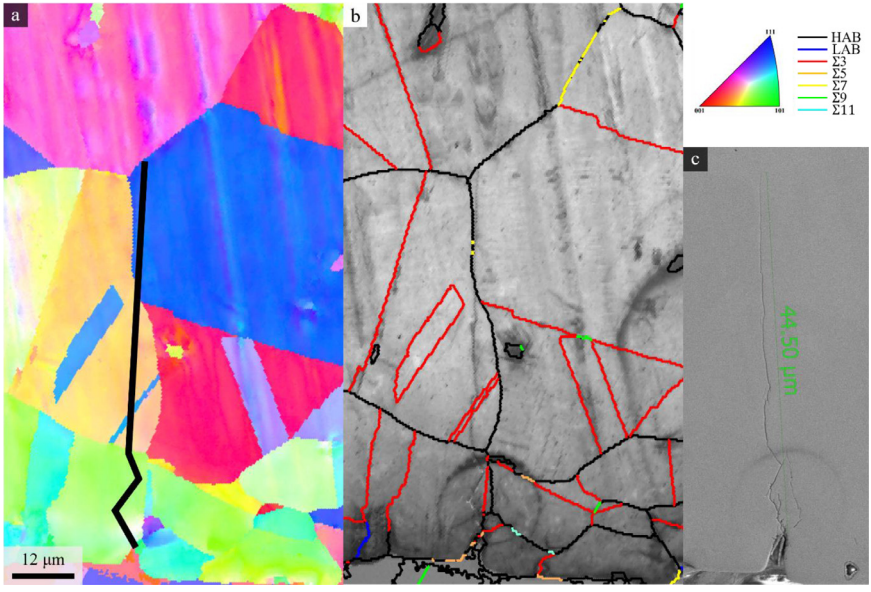


**Fig. 1.** Corresponding (a) IPF, (b) IQ, and (c) SEM images of Crack #11 in the HAZ, illustrating the process for identifying the crack path, which is the black line overlaid on IPF map (a); scale bar is consistent throughout composite figure.

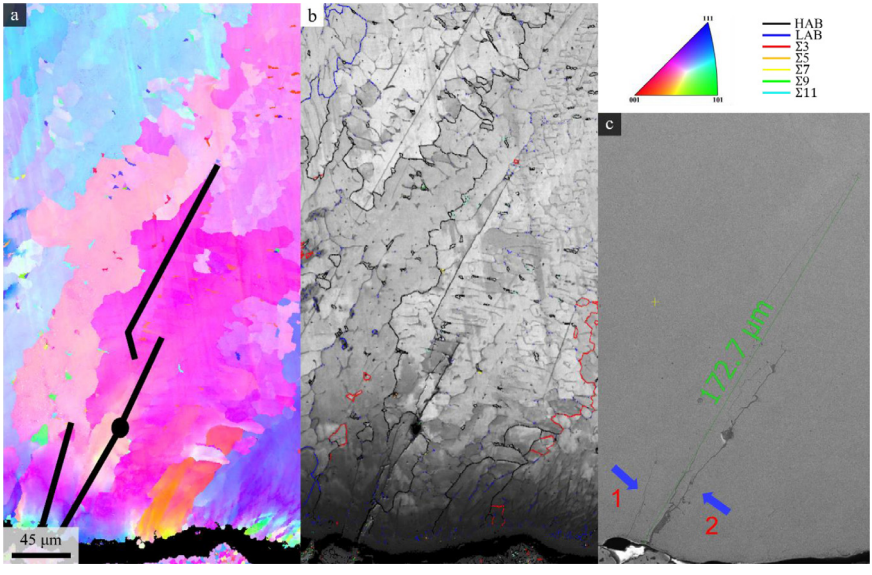


**Fig. 2.** Corresponding (a) IPF, (b) IQ, and (c) SEM images of Crack #29 in the WZ, illustrating the process for identifying the crack path, which is the black line overlaid on IPF map (a); scale bar is consistent throughout composite figure.

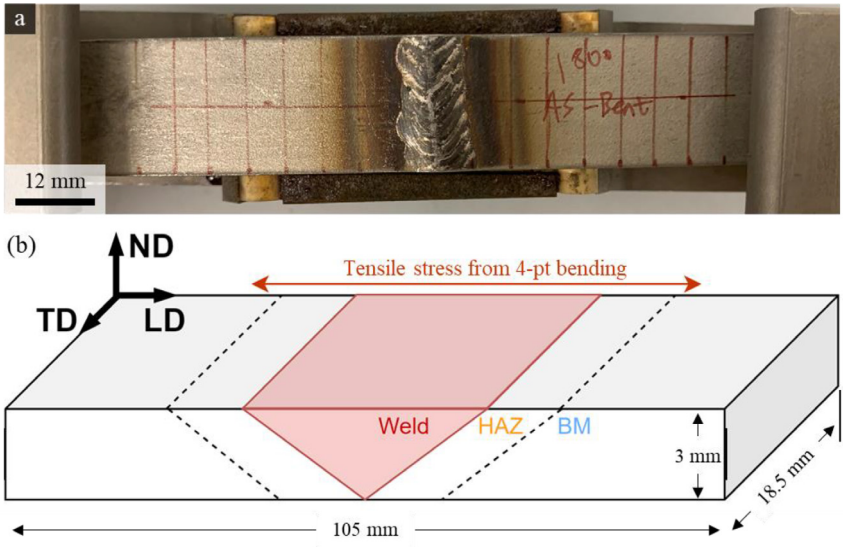


**Fig. 3.** (a) Top view of the as-welded coupon loaded in 4-point bending fixture before SCC testing; (b) schematic diagram of the different zones in the testing coupon.

## 2. Experimental Design, Materials and Methods

### *2.1. Materials and specimen preparation*

Two hot rolled stainless steel (SS) 304L sheets with thickness 3 mm were joined by two-pass gas tungsten arc welding (GTAW) with SS308L filler. The weld was made using a current of 110 A, voltage of 12 V, and interpass temperatures of 23.9°C and 130°C during the first and second passes, respectively. The weld bead was ground flat with a commercial grinding wheel, as shown in Fig. 3**(a)**. An SCC testing coupon was laser cut to dimensions 105 mm × 18.5 mm × 3 mm corresponding to the longitudinal direction (LD), transverse direction (TD), and normal direction (ND), respectively. The weld seam was centered in the LD, Fig. 3**(b)**.

SCC testing was conducted following the ASTM G39 bent-beam method for alloy sheets [1, p. 39]. To introduce tensile stress, the coupon was loaded in a 4-point bending fixture with maximum tensile stress of 380 MPa located on the ground side of the weld seam, Fig. 4. The entire fixture was immersed in boiling magnesium chloride ($MgCl_2$) solution, in the setup shown in Fig. 5. The $MgCl_2$ solution was made by mixing reagent-grade magnesium chloride hexahydrate flake ($MgCl_2$•$6H_2O$) to deionized water to yield a $MgCl_2$ concentration of 54.3%. A heating unit maintained the $MgCl_2$ solution at 155.0 ± 1.0°C (311.0 ± 1.8°F) throughout SCC testing. Every 2 hours, the fixture was removed from $MgCl_2$ solution, cleaned, and the specimen was checked for evidence of pitting or cracking using an optical microscope. SCC testing continued until a through-crack was observed on the sample surface after 17 hours of boiling, Fig. 6.

To prepare the specimen for EBSD analysis, a diamond saw was used to section a specimen from the cracked region, as marked by the blue box in Fig. 6**(c)**. This sectioned piece was metallographically mounted on the cross-section in a conductive Cu mount. The cross-section of the EBSD specimen was sequentially polished using SiC paper from 360 to 1200 grit, followed by 6 $\mu$m, 3$\mu$m, and 1$\mu$m diamond suspension, and finally finished by vibratory polishing with 0.05 $\mu$m colloidal silica.

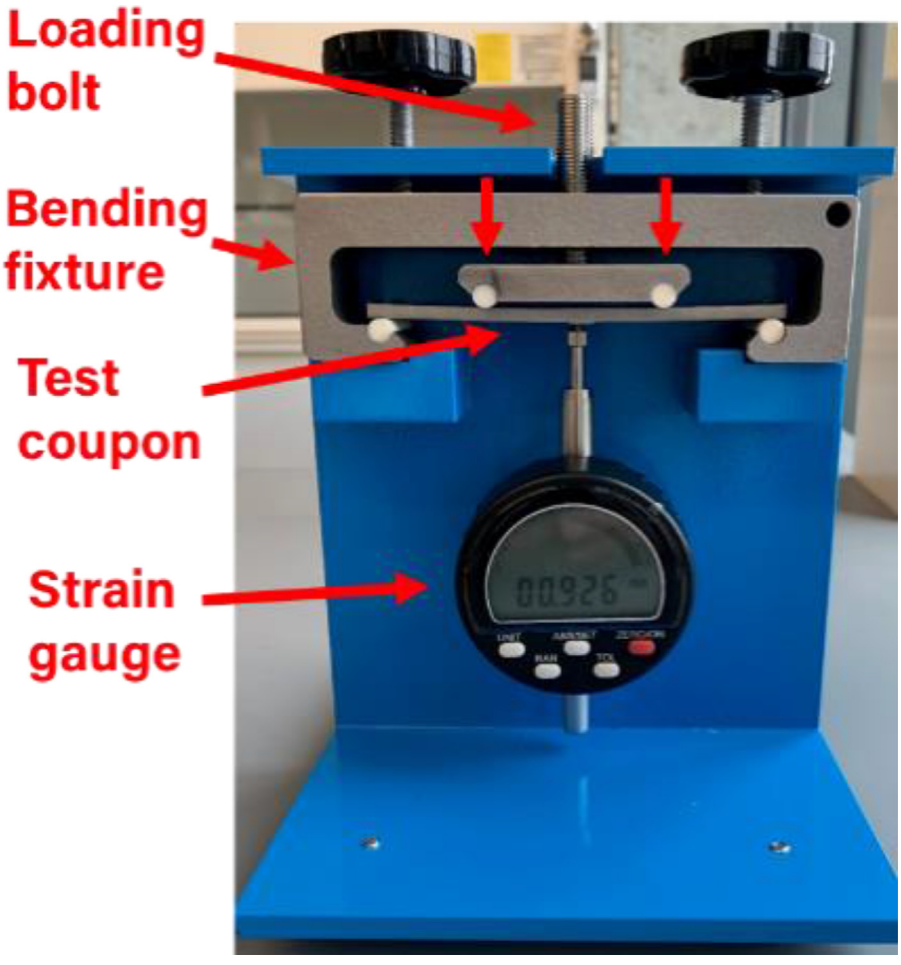


**Fig. 4.** Four-point bending fixture and setup.

### 2.2. SEM-EBSD analysis

The polished EBSD specimen was examined in an FEI (now Thermo Fisher Scientific) Helios G4 UX Dual Beam SEM operating at 5 kV, 0.4 nA, and 4.2 mm working distance for high-resolution (HR) crack morphology imaging. A total of 37 cracks of interest were selected for serial EBSD analysis along the crack path; of these cracks, 10 were in the weld zone (WZ) and 27 were in the heat-affected zone (HAZ).

Serial EBSD mapping was conducted using an FEI Quanta 650 FEG SEM equipped with an EDAX HikariTM EBSD detector [2]. The setup configurations for EBSD mapping were: acceleration voltage of 20kV, spot size 5.5, 15 mm working distance, 70° tilt, 1 ms dwell time, 0.3-2.5 $\mu$m/pixel step size, and neighboring confidence index (CI) $>$ 0.1. A total of 20 serial EBSD maps were generated for all 37 cracks of interest (in some cases, two or more cracks were in close proximity to one another that they could be captured in one serial EBSD map).

Post-EBSD analysis was performed using the EDAX OIM V8 software. Because of debris on the sample surface, EBSD maps contained un-indexable points or points that did not belong to any grain. Grain dilation was used as a cleanup method built in to the EDAX OIM software to

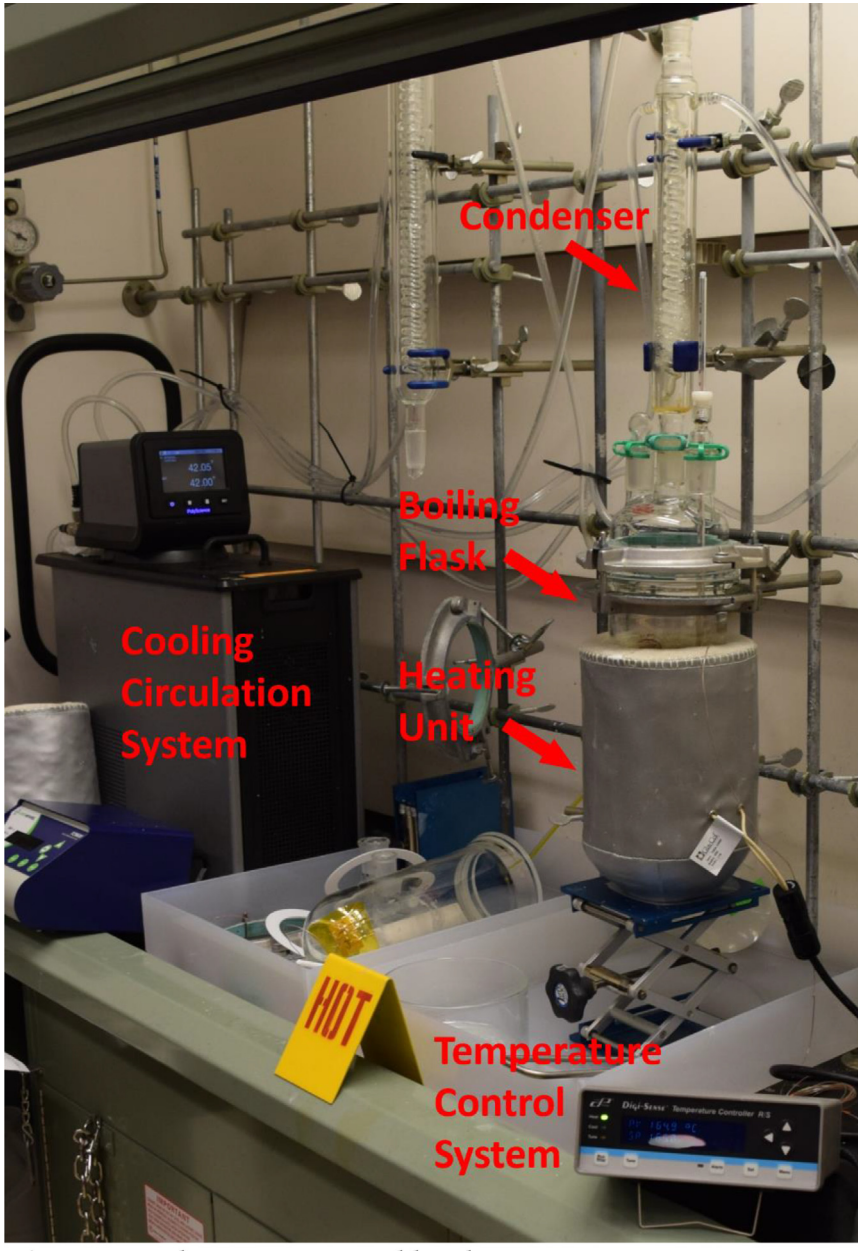


**Fig. 5.** Boiling magnesium chloride corrosion test setup.

match these isolated points to neighboring grains. For the cleanup process, the grain tolerance angle was set to be 3° and the minimum confidence index was set to be 1. Overall, grain dilation cleaned up ~3-10% of all data points within each EBSD map.

The IPF image, IQ figure, SEM detector signal image, and the Taylor and Schmid factors map were generated from each serial EBSD map along the crack paths. Crystal directions in the IPF

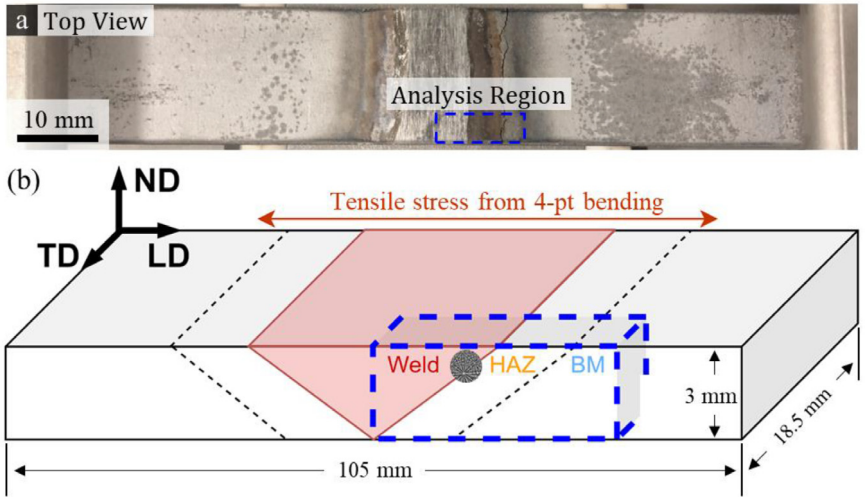


**Fig. 6.** (a)(b) Top view and side view of the cracked coupon after SCC testing; (c) schematic diagram of the testing coupon with blue dashed lines indicating EBSD analysis region.

images were colored normal to the specimen surface (LD-ND plane). In the IQ figures, low-angle grain boundaries (LAB) with misorientation <15°, high-angle grain boundary (HAB) with misorientation between 15° and 180°, and coincidence site lattice (CSL) boundaries were marked. The Taylor factor and Schmid factor of each grain were calculated for 12 potential (1 1 1)[1 $\bar{1}$ 0] slip systems, and the Cauchy strain tensor for uniaxial tension parallel to the longitudinal direction was applied Section 1. has described techniques for handling and working with all of these maps.

## Ethics Statement

The authors followed universally expected standards for ethical behavior in conducting and publishing scientific research.

## CRediT Author Statement

**Haozheng Qu:** Conceptualization, Methodology, Investigation, Formal Analysis, Visualization, Validation, Writing- Original draft; **Janelle P. Wharry:** Conceptualization, Validation, Writing – review & Editing, Resources, Supervision, Funding acquisition.

## Declaration of Competing Interest

The authors declare that they have no known competing financial interests or personal relationships which have or could be perceived to have influenced the work reported in this article.

## Data Availability

Crystallographic orientation data from chloride-induced stress corrosion crack (CISCC) paths in gas tungsten arc welded (GTAW) austenitic stainless steel 304L (Original data) (Mendeley Data).

## Acknowledgments

This work was sponsored by the US Department of Energy – Office of Nuclear Energy through contract DE-NE0008759. The authors are grateful to Dr. Keyou Mao of Oak Ridge National Laboratory for advice on image processing. The authors also acknowledge Dr. Talukder Alam at Purdue University for assistance with SEM-EBSD.

## Supplementary Materials

Supplementary material associated with this article can be found in the online version at doi:10.1016/j.dib.2022.108059.

## References

[1] G01 Committee, "G-39: Practice for Preparation and Use of Bent-Beam Stress-Corrosion Test Specimens," ASTM International. doi: 10.1520/G0039-99R16.

[2] K.S. Mao, et al., Grain orientation dependence of nanoindentation and deformation-induced martensitic phase transformation in neutron irradiated AISI 304L stainless steel, Materialia 5 (Mar. 2019) 100208, doi:10.1016/j.mtla.2019.100208.